Kidney International, Vol. 51 (1997), pp. 1818–1830

Cholesterol feeding accentuates the cyclosporine-induced elevation of renal plasminogen activator inhibitor type 1

CARLA DUYMELINCK, SIMONNE E.H. DAUWE, ETIENNE J. NOUWEN, MARC E. DE BROE, and GERT A. VERPOOTEN

Department of Nephrology-Hypertension, University of Antwerp, Belgium

Cholesterol feeding accentuates the cyclosporine-induced elevation of renal plasminogen activator inhibitor type 1. Long-term cyclosporine (CsA) therapy is accompanied by the occurrence of hypercholesterolemia and renal interstitial fibrosis. The present study investigates the effect of dietary cholesterol on CsA-induced lipid disturbances in the rat and on CsA nephrotoxicity. Since plasminogen activator inhibitor type 1 (PAI-1) is a major inhibitor of matrix degradation and elevated plasma PAI-1 levels are reported to be associated with increased low-density lipoprotein (LDL) cholesterol, PAI-1 was examined in the kidneys of rats fed a sodium-deficient diet, with or without cholesterol. After nine weeks, both diet groups were subdivided into a CsA-treated group and a vehicle-treated group. Although cholesterol feeding significantly aggravated CsA-induced renal function impairment, CsA-induced histological lesions were comparable in both diet groups. Cholesterol feeding significantly decreased high-density lipoprotein (HDL) cholesterol irrespective of the treatment, while CsA treatment significantly elevated serum triglycerides irrespective of the diet. Cholesterol feeding alone did not increase the number of infiltrating cells in the renal interstitium. In contrast, in both diet groups CsA treatment caused a significant influx of macrophages, while combined treatment with CsA and cholesterol additionally elevated the number of T-helper cells in the cortex. In all rats, PAI-1 immunostaining was found mainly in intracellular vesicles (lysosomes) in proximal tubules, which stained most intensely in fibrotic areas of kidneys from CsA-treated rats. Cholesterol feeding enhanced the CsA-induced elevation of renal PAI-1 immunostaining to a significant level. These results show that, although serum creatinine, PAI-1 staining and T cell influx were significantly increased in the cholesterol-fed CsA-treated group compared to the other groups, renal CsA-induced histological lesions were not influenced by cholesterol feeding after short-term (3 weeks) CsA administration. To what extent the more pronounced proximal tubular PAI-1 (inhibitor of matrix degradation) immunostaining in fibrotic areas in the cortex of cholesterol-fed CsA-treated rats contributes to the progression of CsA-induced renal fibrosis remains to be determined.

Since the introduction of CsA into clinical practice, it has become apparent that nephrotoxicity significantly limits its use in transplantation and in the treatment of autoimmune diseases [1]. Transient acute renal failure can be reversed after reduction or discontinuation of CsA therapy [2]. More problematic is the irreversible chronic form of CsA nephrotoxicity [1–4]. Chronic CsA-induced pathological changes in the human kidney include tubular atrophy, cellular infiltration of the renal interstitium, striped cortical interstitial fibrosis and prominent vascular injury, the so-called CsA-associated arteriolopathy [3–6]. These lesions can be reproduced in different normotensive rat strains [7–11]. Application of salt depletion protocols (sodium-deficient diets [12] or furosemide administration [13]) before and during CsA treatment accelerates the development of chronic CsA-induced lesions in the rat [7–11].

In the rat and in humans, irreversible striped cortical fibrosis is the major chronic CsA-induced lesion [1–11]. Tubulointerstitial fibrosis is the net result of increased extracellular matrix (ECM) deposition and/or diminished ECM degradation. Two ECM degrading proteolytic systems, the plasminogen activator (PA)/plasmin system and the matrix metalloproteinase system are likely candidates to participate in matrix turnover to maintain renal interstitial integrity. The PA/plasmin cascade can be blocked at different levels. Although PAs can form complexes with several members of the serine protease inhibitor (serpin) superfamily, the main physiological PA inhibitor is PA inhibitor type 1 (PAI-1), a glycoprotein produced by a variety of cell types [14, 15]. Blockage of plasminogen activation by PAI-1 will inhibit all subsequent plasmin-mediated actions, that is, activation of pro-matrix metalloproteinases and matrix degradation.

CsA-induced hypercholesterolemia aroused interest since Ballantyne et al [16] reported increased plasma cholesterol levels in amyotrophic lateral sclerosis patients on CsA therapy. CsA-associated lipid disturbances in humans include increased triglyceride and total cholesterol levels as well as increases in very-low-density lipoprotein (VLDL) and low-density lipoprotein (LDL) cholesterol concentrations [17–23]. CsA treatment of rats also induces a significant elevation of LDL cholesterol [24]. In addition, CsA has been reported to have a prooxidant effect on plasma LDL in renal transplant recipients [25, 26]. Oxidized LDL (oxLDL) is cytotoxic to endothelial cells, is chemotactic for circulating monocytes and can inhibit the motility of tissue macrophages [27]. Furthermore, oxLDL is known to induce the synthesis of fibrogenic cytokines and growth factors by macrophages, endothelial and smooth muscle cells [27]. *In vitro*, components of oxLDL can stimulate collagen gene expression in fibroblasts, thus suggesting a direct link between matrix deposition and oxLDL as well [27].

Recently, we and others demonstrated increased plasma PAI-1 levels in cyclosporine-treated renal allograft recipients [23, 28]. These higher systemic PAI-1 levels may contribute to thromboembolic complications and eventually to the impairment of renal

Received for publication August 19, 1996
and in revised form December 18, 1996
Accepted for publication December 18, 1996

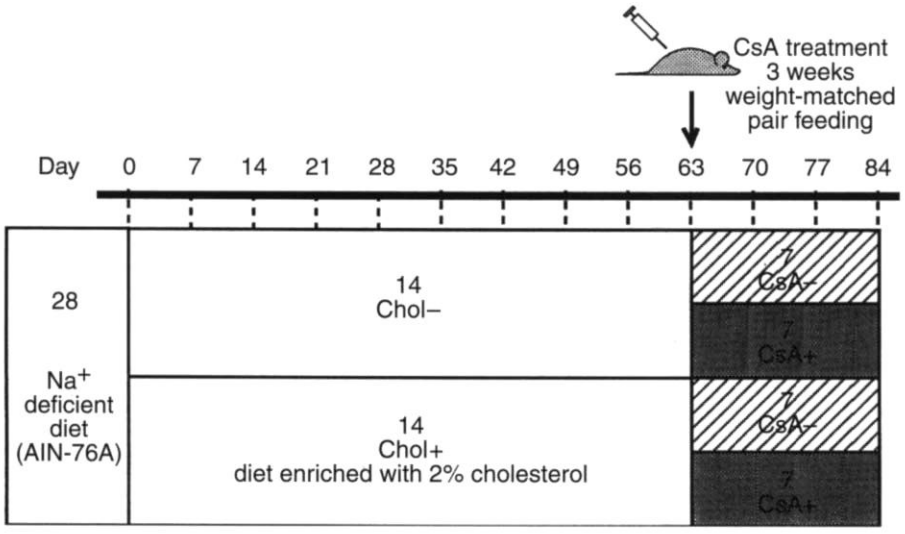

Fig. 1. *Experimental set-up.* Abbreviations are: Chol−, cholesterol-free sodium-deficient diet based on AIN-76A; Chol+, sodium-deficient diet based on AIN-76A supplemented with 2% cholesterol; CsA+, injected daily s.c. with 15 mg CsA/kg body wt; CsA−, injected daily s.c. with an isovolumetric dose of vehicle for CsA (Cremophor EL).

function in CsA-treated patients. The elevation of systemic PAI-1 concentrations may result from the CsA-induced elevation of LDL and VLDL levels, since *in vitro* studies have shown that LDL and VLDL are potent stimulators of PAI-1 release by endothelial cells [29, 30]. A study in mice showed a dramatic increase of (LDL+VLDL) cholesterol after coadministration of CsA and an atherogenic diet [31]. Therefore, we hypothesized that the administration of dietary cholesterol to CsA-treated rats could lead to altered renal PAI-1 levels and an aggravation of renal function impairment compared to CsA treatment alone.

Methods

Experimental model

Twenty-eight male Wistar rats with an initial weight of 200 to 250 g (Janssen Pharmaceuticals, Beerse, Belgium), were housed in individual polypropylene cages under temperature-controlled conditions in a constant dark-light cycle (7.00–19.00 hr light) throughout the entire study period. Food intake and body wt were monitored daily.

The experimental set-up is shown in Figure 1. The animals were randomly assigned to two diet groups: the control diet group (Chol−) received a sodium-deficient diet based on AIN-76A (ICN Pharmaceuticals Inc., San Diego, CA, USA), and the cholesterol-fed group (Chol+) received the same diet supplemented with 2% cholesterol. The diet pretreatment period extended up to nine weeks. After seven weeks, the animals were fasted overnight and serum samples were collected from the tail vein for measurement of serum creatinine levels and total and LDL cholesterol. Nine weeks after initiation of the experiment, the animals were again randomly subdivided into two treatment groups: a CsA-treated group (CsA+) and a vehicle-treated group (CsA−). Before starting the CsA treatment, weight-matched pairs were selected from each treatment group within the same diet group and during CsA treatment, these animals were pair-fed. CsA (SandImmun i.v.; Sandoz Pharmaceuticals Company, Basel, Switzerland) and its vehicle, Cremophor EL (Sandoz Pharmaceuticals Company, Basel, Switzerland) were prediluted in 1 volume of saline solution and sterilized. The CsA+ group received 15 mg CsA/kg body wt daily, injected subcutaneously (s.c.) and the CsA− group received an isovolumetric dose of Cremophor EL, injected s.c. daily.

Before sacrifice, the rats were fasted overnight in metabolic cages. The animals were anesthetized with ether. Blood was drawn by cardiac puncture and partly collected over EDTA for whole blood preparation and partly without additives for serum preparation. Fasted serum samples were stored at −80°C until further use. After prelevation of the rat kidneys, renal capsule and fat tissue were removed, kidneys were rinsed in sterile saline and processed for light microscopy.

Biochemical analyses

CsA trough levels were measured in whole blood with a Fluorescence Polarization Immunoassay (FPIA) with a monoclonal antibody to CsA (TD_x/TD_x FL_x Cyclosporine Monoclonal Whole Blood Assay; Abbott, Louvain-La-Neuve, Belgium). Urinary and serum creatinine were measured using a modified Jaffé colorimetric reaction (Creatinine Merckotest; Diagnostica Merck, Darmstadt, Germany).

Total serum cholesterol was determined with the Monotest Cholesterol CHOD-PAP method (Boehringer Mannheim, Mannheim, Germany). HDL cholesterol was measured after selective precipitation of the LDL and VLDL fractions with polyethylene glycol (Quantolip HDL; Immuno AG, Vienna, Austria). LDL cholesterol levels were determined indirectly by measuring the VLDL+HDL cholesterol fraction after selective LDL precipitation with a solution of dextran sulphate in Tris-HCl, pH 7.4 (Quantolip LDL; Immuno AG). LDL cholesterol was calculated by substracting the (VLDL+HDL) cholesterol from total serum cholesterol values. Serum triglycerides were analyzed enzymatically with a glycerol kinase and a peroxidase dry slide technique, without correction for glycerol (Kodak Ektachem Clinical Chemistry Slides TRIG; Eastman Kodak Company, Rochester, NY, USA).

Morphological lesions

For light microscopy, renal tissue was fixed either in Dubosq-Brazil or formol-calcium fixative and embedded in paraffin. Renal tissue was sectioned at 4 to 5 μm, and periodic acid-Schiff reagent

(PAS) and Sirius stainings were performed on Dubosq-Brazil fixed tissue whereas Masson's trichrome staining was performed on formol-calcium fixed tissue. To minimize variations caused by handling tissue sections, in all instances in which tissues from control and treated animals were compared, tissues were processed and stained in parallel in the same buffers and antibody mixtures.

Tubular damage in the cortex was evaluated in five randomly selected low-power (×100) microscopic fields of PAS or Sirius stained sections (total surface area evaluated per rat 9.6 mm^2). The following lesions were distinguished: (1) tubular atrophy, that is, tubules with decreased diameter, decreased tubular lumen, flattened epithelium, thickened or wrinkled basement membrane and attenuation of the brush border; (2) vacuolization of tubular epithelium; and (3) dilation of tubular lumen. Interstitial fibrosis, defined as areas rich in extracellular matrix and atrophic tubules, was graded semiquantitatively in trichrome stained renal sections using a score system adapted from other groups involved in the study of chronic cyclosporine nephropathy in the rat [7, 32]. Five randomly chosen microscopic fields (magnification 100×) were subdivided into 48 equal squares (total surface area evaluated per rat 9.2 mm^2). Each square received a score from 0 to 3: score 0 was assigned to normal basement membrane staining; score 1 was given to squares containing less than 50% fibrotic tissue; score 2 was given to square sections with more than 50% fibrotic area; and score 3 was assigned to squares entirely filled with atrophic tubules and extracellular matrix. The mean of the scores given to 240 evaluated squares was calculated per rat and the results were expressed as fibrosis score per square. Sections were evaluated without knowledge of the group affiliation of the individual rat.

Cellular proliferation

In order to evaluate cellular proliferation and to localize proliferating cells, PAS was combined with immunostaining for the proliferating cell nuclear antigen (PCNA [33]) using the PC10 monoclonal antibody (DAKO, Denmark) on methacarn-fixed renal tissue. All PCNA-positive nuclei within 20 randomly selected cortical microscopic fields were counted (magnification ×200, total surface area evaluated per rat 9 mm^2). Proliferation was examined separately in intact tubules, in damaged tubules (atrophic tubules, tubules with dilated lumen and tubules with vacuolized epithelial cells), in glomeruli and in the renal cortical interstitium. At least 40 glomerular cross sections were evaluated per rat. Results were expressed as absolute numbers of PCNA+ cells per mm^2 cortex or per glomerular cross section. Sections were evaluated without knowledge of the group affiliation of the individual rat.

Phenotyping of interstitial inflammatory cells

Pan-leukocyte and macrophage stainings were performed on methacarn-fixed, paraffin-embedded renal tissue. Leukocytes were stained with the OX-1 monoclonal antibody (Serotec, Oxford, UK) that recognizes the rat leukocyte common antigen (LCA) present on all marrow-derived leukocytes, that is, thymocytes, bone marrow cells, peripheral lymphocytes and macrophages [34]. Macrophages were identified with the ED1 monoclonal antibody (Serotec), which is directed to a cytoplasmic antigen of monocytes and tissue macrophages, but also recognizes dendritic cells [35]. Immunohistochemical detection of lymphocytes was performed on 5 μm renal tissue cryosections prefixed in formol-calcium. The W3/25 monoclonal antibody (Serotec) used to detect T-helper cells is directed to the rat CD4-equivalent [36]. The OX-8 monoclonal antibody (Serotec) was used to detect T-suppressor/cytotoxic and natural killer cells, and is directed to the rat CD8-equivalent [36]. B lymphocytes were counted in sections stained with the OX-4 monoclonal antibody (Harlan Sera-Lab Ltd., Sussex, UK), which recognizes the Ia marker present on B cells and dendritic cells [37]. Nuclei were counterstained with methyl green.

Cells showing distinct immunoreaction were counted in 10 randomly chosen areas (magnification ×200, total surface area evaluated per rat 4.5 mm^2) in the superficial cortex, and in 10 random areas in the deeper cortical area. Per renal section at least 25 glomerular profiles were examined for infiltrating cells. Inflammatory cells not contained within large blood vessels or glomerular cross sections were considered to be interstitial. Results were expressed as absolute numbers of immunoreactive cells per mm^2 or per glomerular cross section. Sections were evaluated without knowledge of the group affiliation of the individual rat.

Immunohistochemical staining for PAI-1

Renal tissue fixed in formol-calcium and embedded in paraffin was sectioned at 4 μm and mounted on poly-L-lysine coated microscope slides, deparaffinized and rehydrated. To unmask PAI-1 antigens, renal sections were incubated at room temperature with a 0.003% solution of trypsin III (Sigma Chemie, Bornem, Belgium) in 0.01 M Tris-HCl, pH 7.3, in 0.9% NaCl containing 1 mM $CaCl_2$ and washed with Tris saline buffer (TSB: 10 mM Tris-HCl, pH 7.6, 0.9% NaCl, 0.1% Triton X-100 and 0.004% merthiolate). Mouse anti-human PAI-1 monoclonal antibody, MA-7F5 (provided by Dr. R.H. Lijnen and Dr. P. Declerck, Center for Molecular and Vascular Biology, Leuven, Belgium [38]) was applied for overnight incubation. After washing in TSB, sections were treated with methanol and 0.03% H_2O_2 to quench endogeneous peroxidase activity, and incubated with biotinylated horse anti-mouse serum (ABC kit; Vector Laboratories Inc., Burlingame, VT, USA). To prevent a cross-reaction of horse anti-mouse serum with rat IgG, 5% normal rat serum was added to the secondary antibody mixture 30 minutes before use. After washing in TSB, the avidin-biotin peroxidase complex (ABC kit; Vector Laboratories Inc.) was added and color development was performed with AEC as chromogen in the presence of 0.006% H_2O_2. Controls for background staining were obtained by performing parallel stainings in which the primary antibody was omitted. Specificity of the primary antibody was examined by staining with normal mouse serum in different dilutions, and confirmed in pre-adsorption experiments on serial sections in which purified PAI-1 antigen of human origin (PAI-1 antigen standard, Innotest PAI-1; Innogenetics, Ghent, Belgium) was added to the antibody solution in a final concentration ranging from 2.5 to 50 ng/ml and incubated for one hour at room temperature. To identify PAI-1 immunoreactive cells, PAI-1 immunostaining was combined with PAS histological stain on formol-calcium-fixed renal tissue and the chromogen 3,3′-diaminobenzidene (DAB) was used to visualize antigen-antibody staining.

To evaluate the focal PAI-1 immunostaining, stained sections of all experimental groups were blinded and considered as a single sample for purposes of ranking. The sections were ranked, taking into account a number of factors including: (1) the number of

positive vesicles per microscopic field; (2) vesicle-size; (3) the intensity of the staining; (4) the cortical surface containing PAI-1 immunoreactive vesicles. The section with the weakest PAI-1 immunostaining received rank 1. Sections with more extensive PAI-1 antigen staining were given progressively higher ranks. Ranking was performed by one investigator (CD) on three separate occasions, and by an independent investigator (GV) on a single occasion. The correlation between the repeated rankings and the correlation between the observations of two investigators were high (Rs > 0.91 and Rs > 0.76, respectively, $P < 0.0001$). Therefore, only the results obtained by investigator CD were used for further analysis.

Statistics

Results are expressed as mean ± SD, unless stated otherwise. Differences between the means of two groups were analyzed with the *t*-test for independent samples. Effects of CsA treatment and cholesterol feeding were analyzed with multiple ANOVA (MANOVA), followed by group-to-group comparisons with the Student-Newman-Keuls test with a significance level of 0.05. Ranking data were tested for overall differences using the Kruskal-Wallis test, followed by post-hoc comparison testing using the Mann Whitney *U*-test, significance level 0.05. Spearman's rank correlation test was used to establish correlations (with correlation coefficients Rs). Statistical analysis was computed using two software packages: SPSS (release 6.0) and STATISTICA (release 4.3) for MS Windows.

Results

Body weight and renal function

There was no mortality during the course of the study. Pair-feeding was successful since all animals had comparable body weights at the time of sacrifice. Seven weeks after the initiation of the diet pretreatment, renal function was not influenced by the type of diet as shown by the serum creatinine levels of both diet groups (Chol−, 0.42 ± 0.03 mg/dl vs. Chol+, 0.43 ± 0.06 mg/dl). After three weeks of CsA treatment both CsA+ groups had significantly elevated serum creatinine levels compared to the vehicle-treated groups (Fig. 2). Cholesterol feeding aggravated renal function impairment, as shown by the significantly increased serum creatinine levels in the Chol+CsA+ group, compared to the Chol−CsA+ group. CsA whole blood levels were significantly lower (*t*-test for independent samples, $P < 0.05$) in the Chol+CsA+ group (4562 ± 829 ng/ml) compared to the Chol−CsA+ group (6092 ± 549 ng/ml).

Serum lipids

Feeding rats a sodium-deficient diet supplemented with 2% cholesterol during seven weeks, did not result in an increase of total cholesterol (Chol−, 106.1 ± 25.8 mg/dl vs. Chol+, 97.5 ± 26.9 mg/dl). The LDL cholesterol fraction, however, showed a tendency towards an increase in cholesterol-fed rats (Chol−, 6.4 ± 3.1 mg/dl vs. Chol+, 10.2 ± 9.7 mg/dl). Serum lipids after three weeks CsA or vehicle treatment are represented in Figure 3. Cholesterol feeding significantly decreased the serum HDL cholesterol fraction in both vehicle-treated and CsA-treated rats ($P = 0.0001$). There was a tendency towards an elevation of VLDL and LDL cholesterol levels after CsA treatment, irrespective of the diet administered. VLDL cholesterol levels were significantly increased in the Chol−CsA+ group (Fig. 3). The result of these effects on the different cholesterol fractions was a significant elevation of total cholesterol levels in the Chol−CsA+ group compared to all other groups ($P = 0.0001$). Serum triglycerides levels were significantly increased in both CsA+ groups, and were highest in the Chol−CsA+ group (Fig. 3).

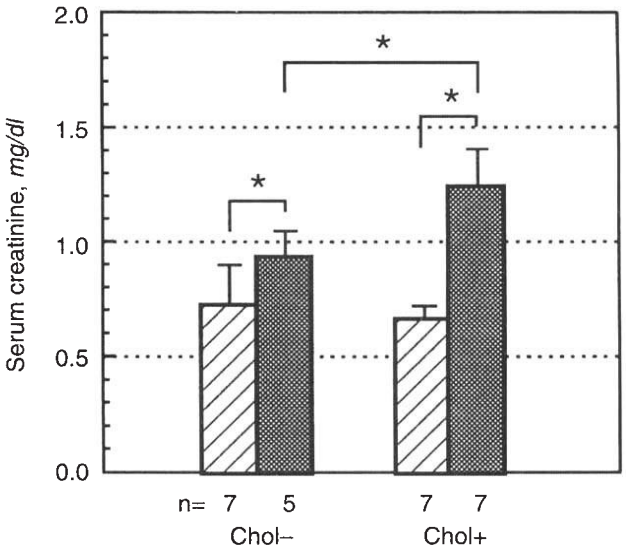

Fig. 2. *Serum creatinine levels (mg/dl) after 3 weeks of CsA treatment (CsA+) or vehicle treatment (CsA−).* A sodium-deficient cholesterol-free diet (Chol−) and a sodium-deficient diet enriched with 2% cholesterol (Chol+) were administered during a period of 9 weeks before the initiation of the CsA treatment and during the CsA treatment. Each bar represents the mean ± SD. Symbols are: (▨) vehicle-treated; (▩) CsA treated; *$P < 0.05$.

Morphological lesions

CsA-induced renal injury was largely confined to the cortical area and consisted of foci of atrophic tubules, surrounded by increased extracellular matrix and inflammatory cells. Most of the atrophic tubules had thick, wrinkled basement membranes. In PAS and trichrome stained sections, epithelial cells of dilated tubules were optically translucent, containing small isometric vacuoles. In the triangular scarred subcapsular areas, tubular basement membranes sometimes lost their integrity, rendering the identification of tubules difficult. Alterations of cells in dilated and atrophic tubules precluded exact classification of the cell type. Tubules with large vacuoles were found adjacent to atrophic foci. Tubular microcalcifications were observed in the medulla of (CsA+)-animals. Some of the superficial fibrotic areas extended towards the inner cortex to form "striped" scarred areas. No glomerular or arterial renal lesions could be detected.

The percentage of atrophic tubules was significantly increased after three weeks of CsA treatment ($P < 0.00001$). An average of 27% of all cortical tubules in kidneys from CsA+ rats were atrophic (Fig. 4). Vacuolization and dilation of tubules (Fig. 4), were significantly increased after CsA treatment ($P < 0.00001$) and were observed in 12% of all cortical tubules of CsA+ rats. Administration of a cholesterol-supplemented diet alone did not cause tubulointerstitial fibrosis. The fibrosis score of both CsA-treated groups was higher than the fibrosis score of both vehicle-treated groups (Fig. 4). CsA-associated renal fibrosis was not

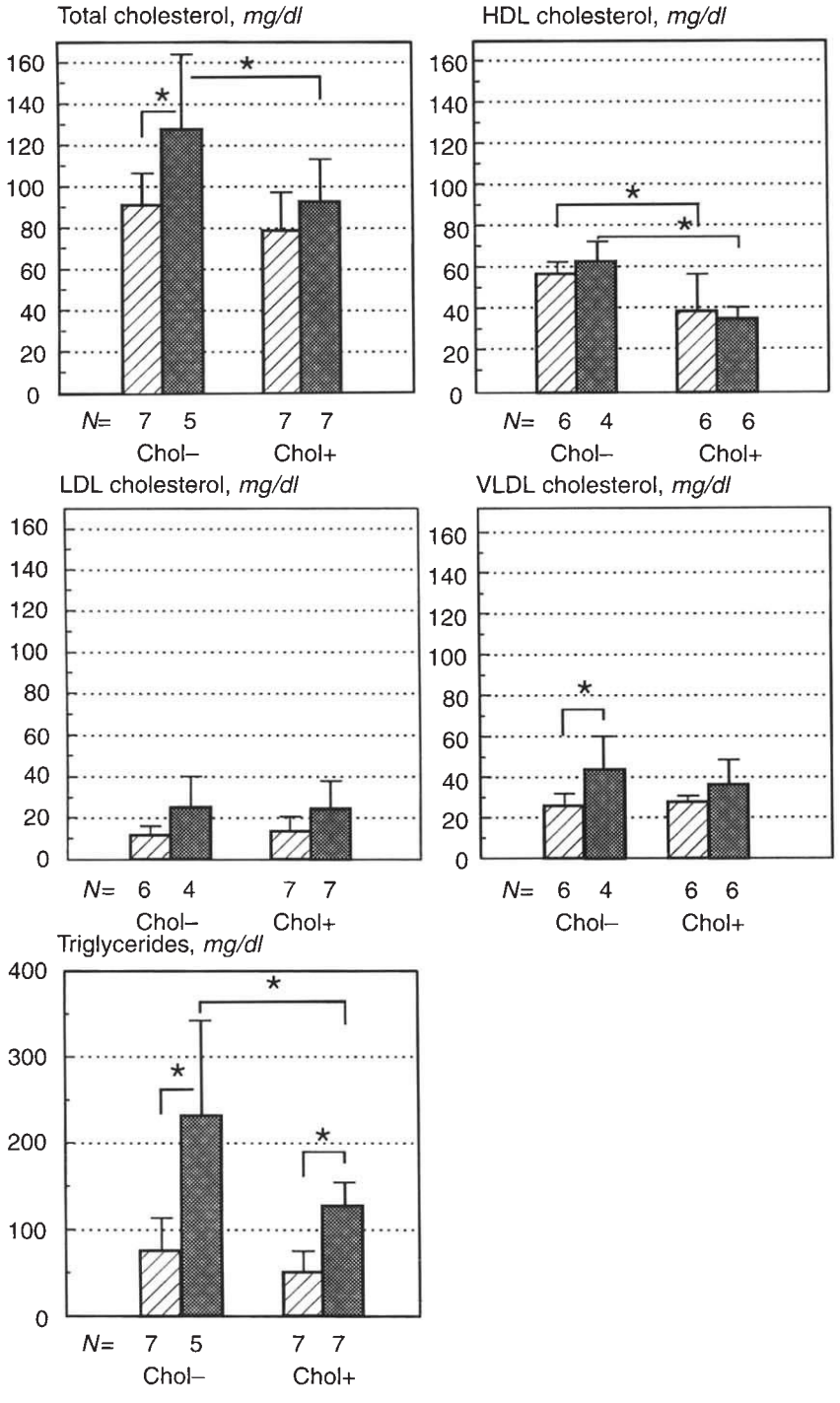

Fig. 3. *Serum lipoprotein cholesterol fractions and serum triglycerides after 3 weeks of treatment with 15 mg CsA/kg body wt (CsA+) or with an isovolumetric dose of Cremophor EL (CsA−).* Each bar represents the mean ± SD. Symbols are: (▨) vehicle-treated; (▩) CsA-treated; *$P < 0.05$. Abbreviations are: Chol−, cholesterol-free sodium-deficient diet; Chol+, sodium-deficient diet supplemented with 2% cholesterol.

aggravated by feeding the rats a diet supplemented with 2% cholesterol during a period of 12 weeks (Fig. 4).

Cellular proliferation

Cellular proliferation (PCNA positivity) was pronounced in the interstitial compartment and in injured tubules in scarred cortical areas of CsA-treated rats, whereas it was almost absent in adjacent intact areas (Fig. 5B). CsA treatment significantly increased the number of PCNA+ cells in injured tubules, that is, atrophic tubules, tubules with vacuolized epithelium and tubules with a dilated lumen (Fig. 6). In intact tubules, cellular proliferation was significantly higher in the Chol−CsA+ group compared to all other experimental groups (Fig. 6). Proliferation of interstitial cells was significantly increased after CsA treatment (Figs.

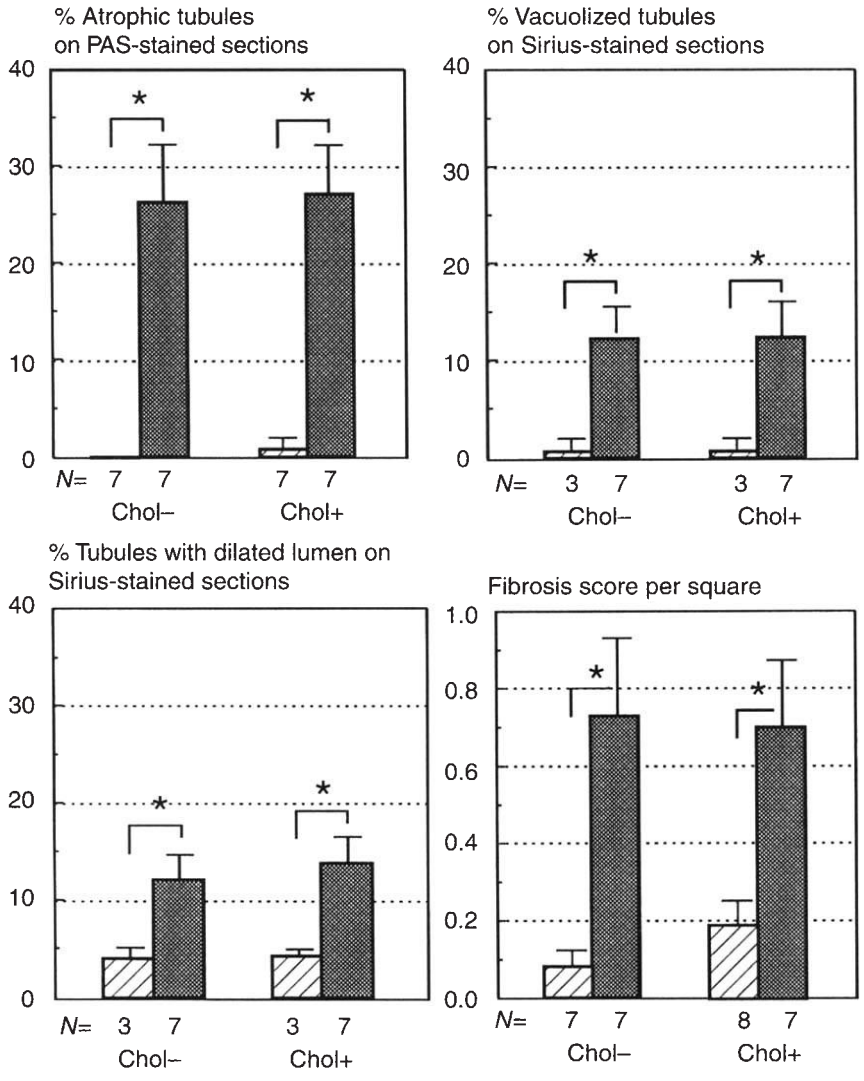

Fig. 4. *Quantification of morphological lesions in the renal cortex and fibrosis score per square.* Tubular atrophy, vacuolization of tubular epithelium and dilation of tubules are expressed as the percentage of damaged tubules. Fibrosis was graded (Masson's trichrome staining) using the following score system: 0 = intact renal tissue; 1 = <50% fibrotic cortical tissue (atrophic tubules and extracellular matrix); 2 = >50% fibrotic tissue; 3 = area completely filled with atrophic tubules and extracellular matrix. Each bar represents the mean ± SD. Symbols are: (▨) vehicle-treated; (▩) CsA-treated; $^*P < 0.05$. Abbreviations are: Chol−, cholesterol-free sodium-deficient diet; Chol+, sodium-deficient diet supplemented with 2% cholesterol.

5 B, C, and 6). CsA significantly increased the number of PCNA+ cells in glomeruli irrespective of the diet treatment, while administration of a cholesterol-supplemented diet during CsA treatment additionally stimulated cell proliferation in the glomerular compartment (Fig. 6).

Phenotyping of inflammatory cells

Although infiltration was slightly higher in the superficial cortex than in deeper cortical areas, significant group-to-group differences were the same in both cortical areas. Therefore, the results were expressed as number of inflammatory cells per mm^2 renal cortex. Kidneys from vehicle-treated rats contained very few ED1 positive cells but much more W3/25 immunoreactive cells (Fig. 7). Dietary cholesterol in itself did not cause an influx of inflammatory cells (Fig. 7). Irrespective of the diet, CsA caused a significant increase of macrophages (ED1+), T-suppressor/cytotoxic cells (OX-8+) and B cells (OX-4+), but the number of T-helper cells (W3/25+) was not significantly increased when CsA was administered alone (Fig. 7). However, when the CsA-treated rats were given a cholesterol-supplemented diet, the number of tubulointerstitial T cells, particularly of T-helper cells, significantly increased in both cortical areas (Fig. 7). Neutrophils were sparse in all four experimental groups. In glomeruli, CsA treatment caused a significant increase of ED1+ cells, which was not influenced by the administration of dietary cholesterol: glomerular cross sections from (CsA+)-rats contained an average of 4 to 6 ED1+ cells.

Immunohistochemical staining for PAI-1

Negative controls, performed by immunostaining in which the primary antibody was omitted or in which normal mouse serum was used as a source of mouse immunoglobulins, produced no signal (data not shown). Pre-adsorption of the primary antibody using increasing amounts of purified human PAI-1 caused immunohistochemical signals to disappear (data not shown). Therefore, the immunohistochemical signals obtained with the monoclonal antibody MA-7F5 can be considered to be specific for PAI-1 antigen.

PAI-1 was immunodetectable in kidneys from all experimental groups. PAI-1 immunoreactive signals were most prominent in the cortex. Immunolocalization of PAI-1 was comparable in both vehicle-treated groups: intense PAI-1 immunoreactive vesicles

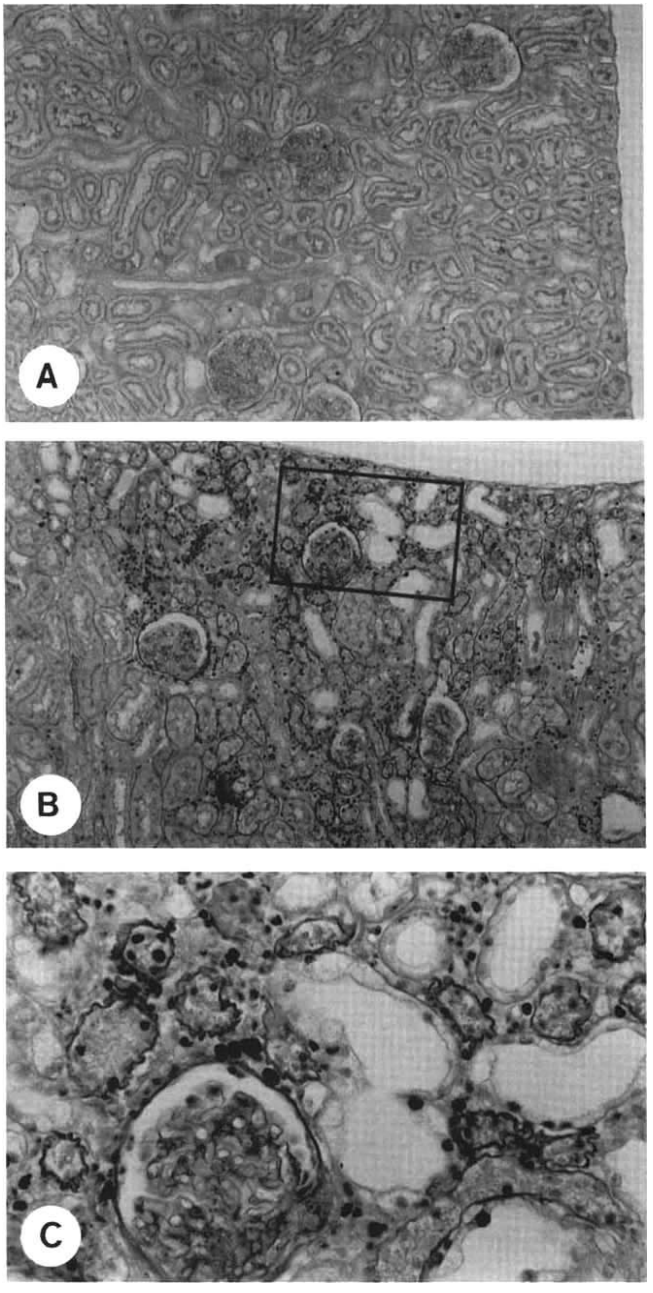

Fig. 5. *PAS/PCNA staining of renal sections of a vehicle-treated cholesterol-fed rat (A) and a CsA-treated cholesterol-fed rat (B, C).* A. The cortex of the vehicle-treated rat contains very few PCNA immunoreactive cells. B. Note the striking PCNA positivity in the damaged tubules and in the interstitial space of a subcapsular injured focus compared to the few PCNA immunoreactive cells found in an adjacent intact area (left hand corner) in the renal cortex of a CsA-treated rat. C. A detail from micrograph B shows PCNA positive nuclei in epithelial cells of atrophic tubules and tubules with a dilated lumen and interstitial cells (magnification A and B, ×80; C, ×281).

were observed in cortical tubules and appeared to be confined to proximal tubular cells (Fig. 8A). Sections stained for the lysosomal enzyme acid phosphatase [39] were compared with PAI-1 stained sections (data not shown). Acid phosphatase and PAI-1 staining demonstrated a comparable intracellular localization. Furthermore, both stainings were more intense in the S1 and S2 portions of the proximal tubuli in the cortex than in the S3 segment in the outer stripe of the outer medulla (Fig. 8B). This suggests that the PAI-1 immunoreactivity has a lysosomal localization. PAI-1 positivity was also found as homogeneous cytoplasmic staining in arterial smooth muscle cells and in visceral epithelial cells (Fig. 8C). As in both vehicle-treated groups, PAI-1 immunoreactivity was present in kidneys of both CsA-treated groups in intracellular vesicles in proximal tubular cells, and as a cytoplasmic staining of arterial smooth muscle cells and visceral epithelial cells. However, three weeks of CsA treatment with or without the administration of dietary cholesterol resulted in more pronounced PAI-1 staining of vesicles in damaged (atrophic, dilated) proximal tubules located within fibrotic areas (Fig. 8D). The majority of the atrophic and dilated tubules in these damaged areas contained large amounts of PAI-1 immunoreactive material within sometimes large vesicles (Fig. 8 D, E); a few of them, however, contained almost no PAI-1 positive vesicles (Fig. 8F). In both CsA-treated groups, PAI-1 immunolocalization was comparable. In a limited number of sections of all four experimental groups, collecting and papillary ducts were stained for PAI-1 at the apical side. Cytoplasmic PAI-1 immunostaining of glomerular and smooth muscle cells, was no longer visible in combined PAI/PAS stainings (Fig. 8F), presumably due to the use of the less sensitive DAB-substrate to visualize antigen-antibody binding.

Semiquantitative analysis of PAI-1 immunostained renal sections showed a tendency towards an increase of PAI-1 staining after CsA treatment that was elevated to a significant level by the administration of dietary cholesterol (Table 1). No effect of cyclosporine treatment and cholesterol feeding on the cytoplasmic staining of both smooth muscle cells and visceral epithelium was found.

Discussion

The CsA-induced tubulointerstitial lesions observed in our model were consistent with those in previously described rat models of chronic CsA nephrotoxicity [7, 9, 11]. After CsA treatment, renal PAI-1 staining showed a tendency towards an increase in fibrotic areas, and dietary cholesterol accentuated this effect to a significant level. In addition, cholesterol feeding aggravated CsA-induced renal function impairment.

Cholesterol feeding alone did not influence renal function, but combined CsA therapy and dietary cholesterol supplementation resulted in more pronounced renal function impairment. CsA mediates renal vasoconstriction through various vasoactive substances including endothelin and thromboxanes [40]. As dietary cholesterol and cholic acid have been shown to enhance renal thromboxane synthesis [41], the combination of CsA and dietary cholesterol may have enhanced thromboxane production compared to CsA treatment alone. The more pronounced decline of renal function in the cholesterol-fed CsA-treated group was not the consequence of higher CsA whole-blood levels. On the contrary, cholesterol feeding resulted in lower CsA whole-blood levels. The lower levels of circulating CsA in the cholesterol-fed CsA-treated group may be due to the cholesterol-induced decrease of serum HDL cholesterol. In blood, up to 80% of CsA is transported in various lipoprotein fractions [42] that are metabolized at different rates [20]. Since CsA preferentially incorporates into triglyceride-poor HDL particles that are metabolized relatively slower than the triglyceride-rich VLDL and LDL particles

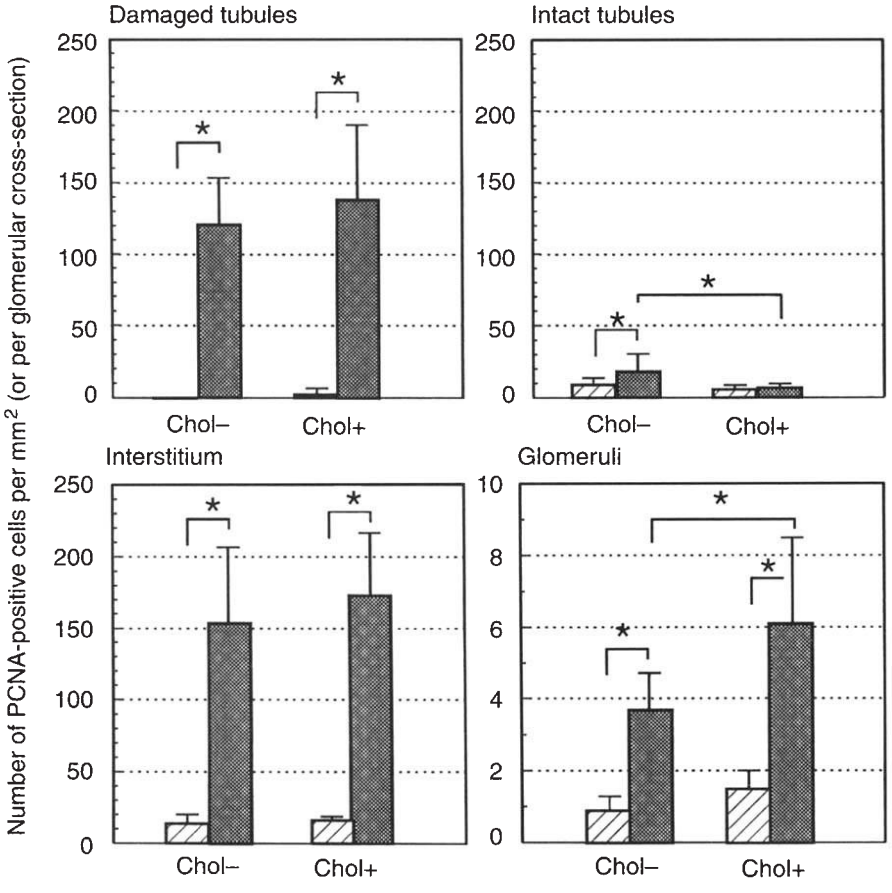

Fig. 6. *Quantification of cell proliferation in the cortex.* Proliferation was quantified separately in CsA-injured tubules (atrophic tubules, dilated tubules and tubules with vacuolized epithelium), in intact tubules, in the cortical interstitial space, and in glomerular cross sections. Results are expressed as the number of PCNA positive cells per mm^2 cortex or per glomerular cross section. Each bar represents the mean ± SD. Symbols are: (▨) vehicle-treated; (▩) CsA-treated; $^*P < 0.05$. Abbreviations are: Chol−, cholesterol-free sodium-deficient diet; Chol+, sodium-deficient diet supplemented with 2% cholesterol. Note the difference in scale in the bar graph representing the data of glomerular PCNA positivity.

[22, 42], high HDL levels may maintain elevated CsA whole-blood levels. On the other hand, dietary cholesterol is known to increase the hepatic transcription of rat 7α-hydroxylase [43], a cytochrome P450 enzyme that shares many features with the mixed-function cytochrome P450 monoxygenases [44]. Since substances interfering with the P450 pathway responsible for the conversion of cholesterol to bile acids also interfere with CsA catabolism, it is possible that dietary cholesterol in turn increased the hepatic expression of cytochrome P450 A3, thereby increasing the catabolism of the CsA molecule. Finally, incorporation of CsA into lipid bilayers is greatly influenced by membrane fluidity. A decreased cholesterol/phospholipid ratio (increased fluidity) favors CsA insertion [45]. However, since total cholesterol levels were not influenced in our experimental setting, it is unlikely that the cholesterol content of cell membranes was altered to a degree in which CsA incorporation was affected.

The aggravation of renal dysfunction after combined treatment with CsA and dietary cholesterol was not reflected by an increase of CsA-induced renal histopathological lesions in our model. In a recent paper, Eddy, Liu and McCulloch [46] studied the effect of pronounced diet-induced hypercholesterolemia on the development of tubulointerstitial fibrosis in the uninephrectomized rat. After 12 weeks, the hypercholesterolemic rats had a significantly increased total kidney collagen content compared to uninephrectomized rats fed standard chow. In our model, in which total cholesterol levels were not increased after cholesterol administration, the lack of differences between the fibrosis score of the diet groups may be due to the limited duration of our experiment.

The significantly increased PCNA positivity of tubular and interstitial cells in focal injured areas in kidneys of CsA-treated rats in our model was in agreement with reports by other groups [7]. However, when rats were given a higher dose of CsA during a shorter period, proliferation (measured as [^{3}H] thymidine incorporation) was reported to be mainly confined to the interstitial compartment [10]. In our experimental setting, CsA stimulated PCNA expression in injured tubules and in the interstitial compartment. Mitotic figures, however, were rarely seen in atrophic or dilated tubules. Since PCNA is an auxiliary protein for DNA polymerase δ and is required for both DNA replication and DNA repair [47], its expression may be a very sensitive indicator of cell repair following CsA-mediated cell injury [48]. The atrophic and dilated tubules that show extensive PCNA positivity in our model may have the potential to regenerate after discontinuation of the CsA treatment at this stage. The PCNA immunoreactive interstitial cells are most likely T-helper cells and macrophages, since they were the predominant cell type found in the cortical interstitium of CsA-treated rats. Recently, macrophages have been shown to be capable of proliferating [49]. This was confirmed in our model by double stainings for ED1 and PCNA (data not shown).

Whether leukocyte infiltration precedes the formation of progressive renal injury or whether inflammatory cells are recruited

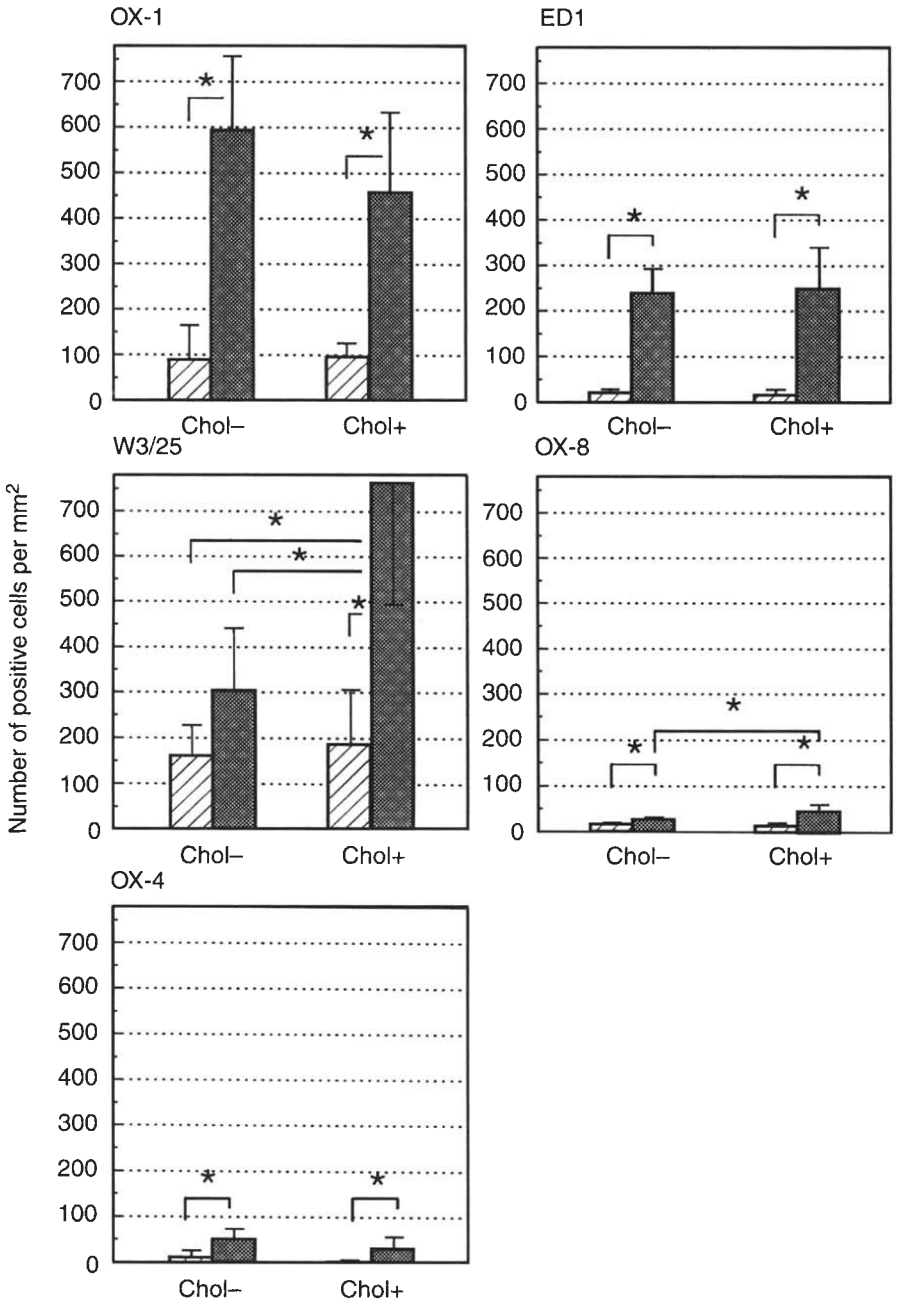

Fig. 7. *Quantification of infiltrating cells in the cortical interstitium.* Results are expressed as the number of immunoreactive cells/mm^2 cortical area. The different inflammatory subsets were identified using the following monoclonal antibodies: OX-1 (leukocytes); ED1 (monocytes/macrophages and dendritic cells); W3/25 (T-helper cells); OX-8 (T-suppressor/cytotoxic cells and natural killer cells); and OX-4 (B lymphocytes and dendritic cells). Each bar represents the mean ± SD. Symbols are (▨) vehicle-treated; (▩) CsA-treated; *$P < 0.05$. Abbreviations are: Chol−, cholesterol-free sodium-deficient diet; Chol+, sodium-deficient diet supplemented with 2% cholesterol.

Fig. 8. *Immunohistochemical PAI-1 staining of formol-calcium-fixed paraffin-embedded renal tissue.* **A, B, D-F:** PAI-1 immunostaining combined with PAS. C: PAI-1 immunostaining with hematoxylin nuclear staining. A-C: Renal sections from a vehicle-treated rat fed a cholesterol-supplemented diet. D-F: Renal sections from a CsA-treated rat fed a cholesterol-supplemented diet. A. PAI-1 immunoreactive vesicles in normal proximal tubular cells. B. PAI-1 positive vesicles in the S1 and S2 segments of the proximal tubules are intensely stained and large (top half of micrograph), while PAI-1 immunostained vesicles in the S3 portion of the proximal tubules are smaller and sparse (arrows, bottom half of the micrograph). C. Cytoplasmic PAI-1 immunostaining in arteriolar smooth muscle cells (large arrows) and in visceral epithelial cells (small arrows). D. Renal cortex of CsA-treated rat. PAI-1 vesicle staining in intact proximal tubules (bottom left corner) is comparable with the PAI-1 staining observed in vehicle-treated rats. Injured tubules contained within fibrotic areas contain large and intensely stained PAI-1 immunoreactive vesicles (arrows). E. Atrophic proximal tubules containing large amounts of intensely stained PAI-1 immunoreactive vesicles, which are sometimes as large as nuclei (arrows). F. Intact proximal tubules in the cortex of a CsA treated rat containing PAI-1 positive vesicles with a comparable size to the PAI-1 immunoreactive vesicles found in proximal tubular cells of a vehicle-treated rat in micrograph A. Some of the atrophic tubules contain very few or no PAI-1 immunoreactive vesicles (arrows) (A, B, E, F, ×414; C, ×1035; D, ×104).

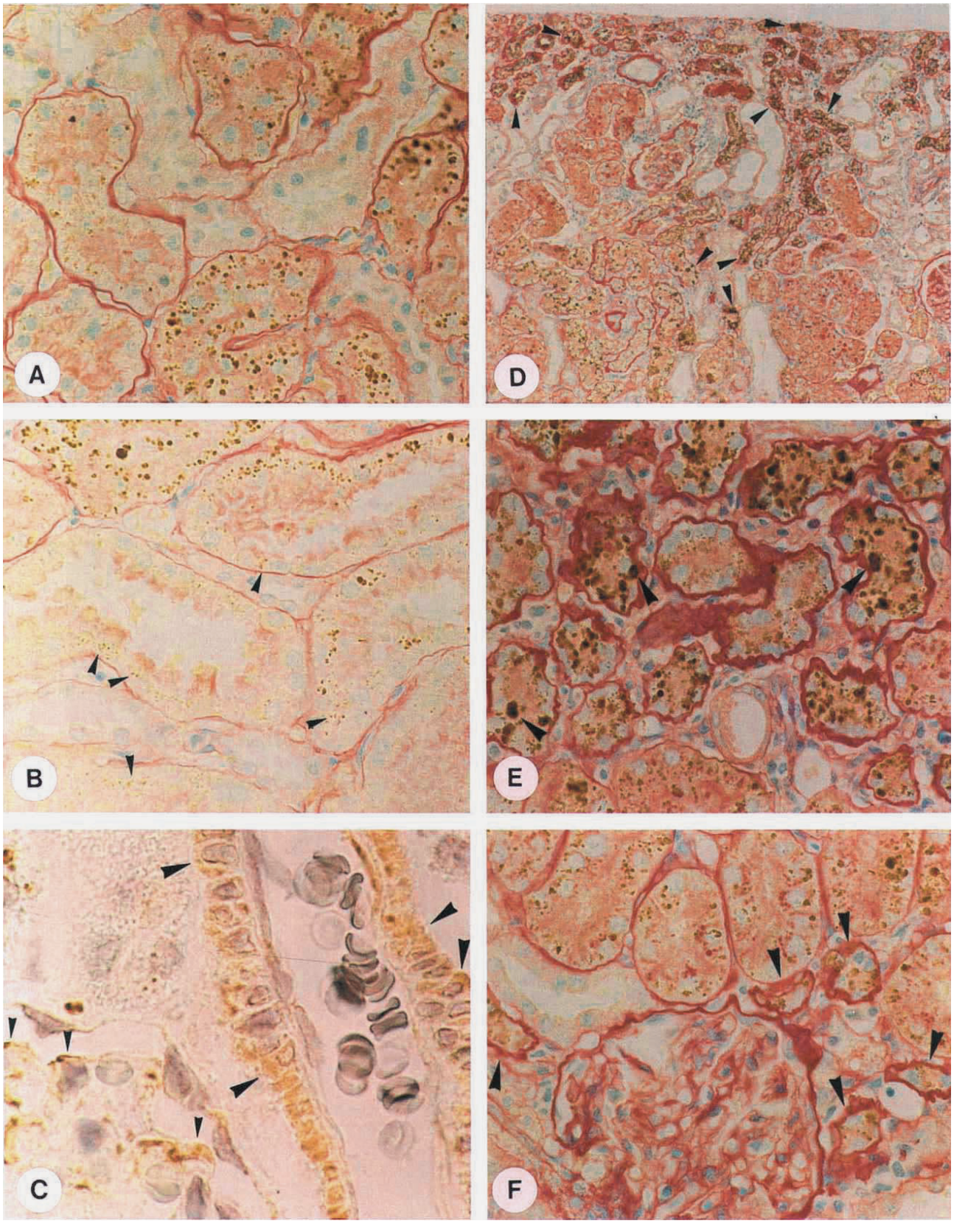

Fig. 8.

Table 1. Ranking of renal sections immunostained for PAI-1

Groups	Mean rank		
	Ranking 1	Ranking 2	Ranking 3
Chol−CsA−	8.5	8.4	8.0
Chol−CsA+	12.4	13.1	13.5
Chol+CsA−	16.5	15.0	15.2
Chol+CsA+	20.6[a,b]	21.5[a,b]	21.3[a]

Ranking was performed on 3 separate occasions (rankings 1, 2 and 3) by researcher CD; ranking data were analyzed for overall differences with the Kruskal-Wallis test and are expressed as mean group ranks. The correlation between repeated rankings was very high: ranking 1 vs. ranking 2, Rs 0.93 ($P < 0.0001$); ranking 1 vs. ranking 3, Rs 0.91 ($P < 0.0001$); ranking 2 vs. ranking 3, Rs 0.97 ($P < 0.0001$).

[a] Significantly different from Chol−CsA− group, $P < 0.05$, Mann-Whitney U-test.

[b] Significantly different from Chol−CsA+ group, $P < 0.05$, Mann-Whitney U-test.

to damaged sites in the kidney, remains to be explored. Young et al [7] observed a striking influx of ED1 immunoreactive cells in the rat kidney as soon as day 5 after initiation of CsA treatment, which preceded cortical fibrogenesis. This suggests that macrophages could play an active role in the progression of CsA-mediated renal scarring since macrophages release a number of factors that promote fibroblast proliferation and collagen synthesis such as TGF-β, IL-1, TNF-α and PDGF [50].

PAI-1 is a local tissue-associated inhibitor of proteolysis, localized at sites of vascular injury or tissue disruption and inflammation. In our experimental setting, PAI-1 antigen was localized in the normal rat kidney in vesicles in proximal tubular cells and in the cytoplasm of visceral epithelium and smooth muscle cells. The following arguments suggest that this staining reflects the actual immunolocalization of PAI-1: (1) negative controls for the staining (omission of the primary antibody and the use of normal mouse serum as source of murine immunoglobulins) produced no immunoreactive signals; (2) pre-adsorption of the primary antibody to increasing amounts of purified human antigen resulted in a progressive decrease of the immunoreactive PAI-1 signals; and (3) the vesicular staining pattern observed in proximal tubular cells could be clearly differentiated from the cytoplasmic staining pattern in visceral epithelial and smooth muscle cells.

Reports on PAI-1 immunostaining of the normal kidney are conflicting. Indirect immunofluorescent PAI-1 staining of human renal tissue, without microscopic abnormalities, revealed strong PAI-1 expression within cytoplasm and foot processes of glomerular cells and weak PAI-1 immunoreactivity in mesangial cells, glomerular capillaries and interstitial cells [51]. Rondeau et al [52], however, reported the absence of significant immunofluorescence with a polyclonal antibody against human PAI-1 in normal human kidneys. Eddy et al [53] were unable to detect PAI-1 antigen in renal tissue from control rats. Using a polyclonal rabbit anti-rat PAI-1 antibody, Tomooka et al [54] and Barnes, Mitchell and Torres [55] detected slight mesangial staining for PAI-1 in the kidneys of untreated Sprague-Dawley rats. In the mouse kidney, renal papilla and medial smooth muscle cells of renal arteries were PAI-1 positive [56]. The discrepancy between our findings and all these observations may be ascribed to species differences, differences in tissue processing, the fact that different antibodies were used as well as different staining techniques, with varying sensitivity. It is conceivable that the use of antibodies directed against different epitopes on PAI-1 could lead to different staining patterns. The antibody used in the present study is able to recognize free (active and latent) and (to a lesser extent) tPA-complexed PAI-1 in human plasma [38]. Since rat PAI-1 is a glycoprotein with a single cysteine residue, no disulfide bridges stabilize its tertiairy structure [57]. Therefore, PAI-1 can adopt different conformations in which neoantigenic epitopes are generated, that is, latent PAI-1 [58], PAI-1 covalently bound to PAs [59] and cleaved inactive substrate PAI-1 [59].

The PAI-1 immunoreactive vesicles are most likely lysosomes since PAI-1 and acid phosphatase (a lysosomal enzyme) have comparable staining patterns. Both stainings are most intense within the S1 and S2 segments of proximal tubules in the cortex, and less pronounced in the S3 segment in the outer stripe of the outer medulla. This corresponds with the fact that rat proximal tubular cells of the S1 and S2 segments have a well-developed vacuolar lysosomal system, while in epithelial cells of the S3 portion of the proximal tubule lysosomes are small and sparse [60]. In addition, lysosomes as large as nuclei have been demonstrated with the acid phosphatase stain in focally distributed proximal tubular cells of CsA-treated rats [39]. This is consistent with the large PAI-1 positive vesicles we found in proximal tubular cells located within fibrotic areas in the cortex of CsA-treated rats. The PAI-1 immunoreactivity observed in proximal tubular lysosomes may consist of internalized PA:PAI complexes. PA:PAI complexes are internalized after binding to the multiligand endocytotic receptor α2-macroglobulin receptor/low density lipoprotein receptor-related protein (α2MR/LRP) [61] or glycoprotein 330 (gp330) in the kidney [62]. In the normal rat kidney, gp330 is mainly expressed by proximal tubular cells [62], the cell type in which the PAI-1 positive vesicles were observed. Furthermore, the expression of gp330 is more pronounced in the S1 and S2 segments than in the S3 segment [62], which is consistent with the more abundant presence of large PAI-1 positive vesicles in the S1 and S2 segments and the lower intensity of PAI-1 vesicle-staining in the S3 portion of the proximal tubule observed in our experimental set-up.

Whether renal PAI-1 observed in vesicles was locally produced or reabsorbed from the filtrate remains to be determined. Free uncomplexed PAI-1 (50 to 54 kDa) [57] may be partially filtered and reabsorbed by proximal tubular cells. However, in plasma, PAI-1 binds to vitronectin, an adhesive glycoprotein that stabilizes PAI in its active conformation [63]. Complexes of PAI-1 with vitronectin and vitronectin multimers (> 150 kDa) [63] are not likely to pass through the glomerular sieve. Furthermore, a pilot rat study conducted by our group showed that plasma PAI-1 levels were not increased after three weeks of CsA treatment (data not shown). Therefore, the PAI-1 observed in proximal tubular cells may be locally synthetized in the kidney. Although PAI-1 mRNA was not detectable in *in situ* hybridizations of control renal tissue of rat and humans [55, 64], Eddy et al [53] and Shihab et al [32] were able to detect PAI-1 mRNA in renal extracts from kidneys from control rats. Furthermore, immunostaining and *in situ* hybridization studies have indicated that tubular cells were the main site of PAI-1 expression within the tubulointerstitium of rats with puromycin aminonucleoside nephrosis [65]. In the protein-overload proteinuria model [53], PAI-1 mRNA expression is significantly increased in kidneys from the proteinuric rats at the time of increased renal matrix protein expression. PAI-1 protein

was immunolocalized in a few cortical tubules and in the wall of large vessels of proteinuric animals, while PAI-1 immunoreactivity was absent in kidneys from control rats [53]. This suggests that at least in this rat model of renal scarring, increased tubular PAI-1 immunostaining was due to increased renal PAI-1 synthesis. In the model of diet-induced hypercholesterolemia in uninephrectomized rats, the increase of PAI-1 gene expression was transient and preceded the development of tubulointerstitial lesions [46]. Finally, Shihab et al [32] demonstrated a progressive increase of renal PAI-1 mRNA expression in rats treated with 15 mg CsA/kg body wt as early as seven days after the initiation of CsA treatment. Based on these data, it is unlikely that the large PAI-1 immunoreactive vesicles observed in injured tubules in the fibrotic cortical areas of CsA-treated rats in our model are composed solely of PAI-1 antigen reabsorbed from the filtrate. Furthermore, in our model, atrophic tubules, which are less functional than intact cells, and dilated tubules, which have a reduced capability to reabsorb due the loss of their brush border, often contain large amounts of PAI-1 positive material.

In summary, in our experimental set-up dietary cholesterol increased CsA-induced renal function impairment, but had no effect on CsA-induced renal histopathological changes in the kidney. Three weeks of CsA treatment caused more pronounced PAI-1 staining in damaged proximal tubules localized within fibrotic areas. Combined cyclosporine treatment and cholesterol feeding accentuated the elevation of PAI-1 immunoreactivity to a significant level. This could implicate a local decrease of intraluminal protein degradation and matrix turnover, and may therefore contribute to the progression of chronic renal scarring in the cyclosporine-treated rat.

Acknowledgments

This study was supported by a grant (G.0218.96), from the Fonds voor Wetenschappelijk Onderzoek. We thank Dr. R.H. Lijnen and Dr. P.J. Declerck (Center for Molecular and Vascular Biology, Leuven) for providing the mouse monoclonal antibody MA-7F5. C. Duymelinck is a recipient of a postgraduate research grant of the "Vlaams Instituut voor de bevordering van het wetenschappelijk-technologisch onderzoek in de industrie (IWT)" (Flemish Institute for the promotion of Scientific Technological Research in Industry). A preliminary report of this work was presented at the 28th Annual Meeting of the American Society of Nephrology at San Diego and published in abstract form (*J Am Soc Nephrol* 6:996, 1995). The authors also express their gratitude to K. Smans for her constructive critisism during the preparation of the manuscript. We also appreciate D. Deweerdt for the excellent illustrations and R. Marijnissen for technical assistance.

Reprint requests to Marc E. De Broe, M.D., Ph.D., University of Antwerp, Department of Nephrology-Hypertension, p/a University Hospital Antwerp, Wilrijkstraat 10, B-2650 Edegem/Antwerp, Belgium.

References

1. Remuzzi G, Dieperink H: Specific drugs-immunosuppression: Cyclosporine/FK506, in *Clinical Nephrotoxicity: Renal Injury from Drugs and Chemicals*, edited by Bennett WM, De Broe ME, Porter GA, Verpooten GA, Dordrecht, Kluwer Academic Publishers Group (in press)
2. Bennet WM, Norman DJ: Action and toxicity of cyclosporine. *Annu Rev Med* 37:215–224, 1986
3. Myers BD: Cyclosporine nephrotoxicity. *Kidney Int* 30:964–974, 1986
4. Myers BD, Ross J, Newton L, Luetscher J, Perlroth M: Cyclosporine-associated chronic nephropathy. *N Engl J Med* 311:699–705, 1984
5. Klintmalm G, Sundelin B, Bohman S-O, Wilczek H: Interstitial fibrosis in renal allografts after 12 to 46 months of cyclosporine treatment: Beneficial effect of low doses in early post-transplantation period. *Lancet* i:950–953, 1984
6. Mihatsch MJ, Thiel G, Spichtin HP, Oberholzer M, Brunner FP, Harder F, Olivieri V, Bremer R, Ryffel B, Stöcklin E, Torhorst J, Gudat F, Zollinger HU, Loertscher R: Morphological findings in kidney transplants after treatment with cyclosporine. *Transplant Proc* 15:2821–2835, 1983
7. Young BA, Burdmann EA, Johnson RJ, Alpers CE, Giachelli CM, Eng E, Andoh T, Bennett WM, Couser WG, Lindsey J, Duyn J: Cellular proliferation and macrophage influx precede interstitial fibrosis in cyclosporine nephrotoxicity. *Kidney Int* 48:439–448, 1995
8. Rosen S, Greenfeld, Z, Brezis M: Chronic cyclosporine-induced nephropathy in the rat. *Transplantation* 49:445–452, 1990
9. Gillum DM, Truong L, Tasby J, Migliore P, Suki WN: Chronic cyclosporine nephrotoxicity. *Transplantation* 46:285–292, 1988
10. Jackson NM, Hsu C-H, Visscher GE, Venkatachalam MA, Humes HD: Alterations in renal structure and function in a rat model of cyclosporine nephrotoxicity. *J Pharmacol Exp Ther* 242:749–756, 1987
11. Dieperink H, Kemp E, Starklint H: Cyclosporine A in high dosages induces renal interstitial fibrosis in the rat. *Transplant Proc* 20:525–527, 1988
12. Gerkens JF, Bhagwandeen SB, Dosen PJ, Smith AJ: The effect of salt intake on cyclosporine-induced impairment of renal function in rats. *Transplantation* 38:412–417, 1984
13. Whiting PH, Cunningham C, Thomson AW, Simpson JG: Enhancement of high dose cyclosporin A toxicity by furosemide. *Biochem Pharmacol* 33:1075–1079, 1984
14. Vassalli J-D, Sappino A-P, Belin D: The plasminogen activator/plasmin system. *J Clin Invest* 88:1067–1072, 1991
15. Scully MF: Plasminogen activator-dependent pericellular proteolysis. *Br J Haematol* 79:537–543, 1991
16. Ballantyne CM, Podet EJ, Patsch WP, Harati Y, Appel V, Gotto AM, Young JB: Effects of cyclosporine therapy on plasma lipoprotein levels. *JAMA* 262:53–56, 1989
17. Druëcke TB, Abdulmassih Z, Lacour B, Bader C, Chevalier A, Kreis H: Atherosclerosis and lipid disorders after renal transplantation. *Kidney Int* 39(Suppl 31):S24–S28, 1991
18. Raine AEG, Carter R, Mann JI, Morris PJ: Adverse effects of cyclosporin on plasma cholesterol in renal transplant recipients. *Nephrol Dial Transplant* 3:458–463, 1988
19. Schorn TF, Kliem V, Bojanovski D, Repp H, Bunzendahl H, Frei U: Impact of long-term immunosuppression with cyclosporin A on serum lipids in stable renal transplant recipients. *Transplant Int* 4:92–95, 1991
20. Webb AT, Plant M, Reaveley D, O'Donnell M, Luck VA, O'Connor B, Seed M, Brown EA: Lipid and lipoprotein(a) concentrations in renal transplant recipients. *Nephrol Dial Transplant* 7:636–641, 1992
21. Edwards BD, Bhatnagar D, Mackness MI, Gokal R, Ballardie FW, Chalmers RJG, Durrington PN: Effect of low-dose cyclosporin on plasma lipoproteins and markers of cholestasis in patients with psoriasis. *Quart J Med* 88:109–113, 1995
22. Kuster GM, Drexel H, Bleisch JA, Rentsch K, Pei P, Binswanger U, Amann FW: Relation of cyclosporine blood levels to adverse effects on lipoproteins. *Transplantation* 57:1479–1483, 1994
23. Verpooten GA, Cools FJ, Van der Plancken MG, Bedert LC, Claes R, Van Gaal LF, De Broe ME: Elevated plasminogen activator inhibitor levels in cyclosporin-treated renal allograft recipients. *Nephrol Dial Transplant* 11:347–351, 1996
24. López-Miranda J, Vilella E, Pérez-Jiménez F, Espino A, Jiménez-Perepérez JA, Masana L, Turner PR: Low-density lipoprotein metabolism in rats treated with cyclosporine *Metabolism* 42:678–683, 1993
25. Sutherland WHF, Walker RJ, Ball MJ, Stapley SA, Robertson MC: Oxidation of low density lipoproteins from patients with renal failure or renal transplants. *Kidney Int* 48:227–236, 1995
26. Apanay DC, Neylan JF, Ragab MS, Sgoutas DS: Cyclosporine

increases the oxidizability of low-density lipoproteins in renal transplant recipients. *Transplantation* 58:663–669, 1994
27. WITZTUM JL, STEINBERG D: Role of oxidized low density lipoprotein in atherogenesis. *J Clin Invest* 88:1785–1792, 1991
28. LEVI M, WIMINK J, BÜLLER HR, SURACHNO J, TEN CATE JW: Impaired fibrinolysis in cyclosporin-treated renal transplant patients. *Transplantation* 54:978–983, 1992
29. TREMOLI E, CAMERA M, MADERNA P, SIRONI L, PRATI L, COLLI S, PIOVELLA F, BERNINI F, CORSINI A, MUSSONI L: Increased synthesis of plasminogen activator inhibitor-1 by cultured human endothelial cells exposed to native and modified LDLs. A LDL receptor independent phenomenon. *Arterioscler Thromb* 13:338–346, 1993
30. STIKO-RAHM A, WIMAN B, HAMSTEN A, NILSSON J: Secretion of plasminogen activator inhibitor-1 from cultured human umbilical vein endothelial cells is induced by very-low-density lipoprotein. *Arteriosclerosis* 10:1067–1073, 1990
31. EMESON EE, SHEN M-L: Accelerated atherosclerosis in hyperlipidemic C57BL/6 mice treated with cyclosporin A. *Am J Pathol* 142: 1906–1915, 1993
32. SHIHAB FS, ANDOH TF, TANNER AM, NOBLE NA, BORDER WA, FRANCESCHINI N, BENNETT WM: Role of transforming growth factor-β1 in experimental chronic cyclosporine nephropathy. *Kidney Int* 49:1141–1151, 1996
33. GARCIA RL, COLTRERA MD, GOWN AM: Analysis of proliferative grade using anti-PCNA/cyclin monoclonal antibodies in fixed, embedded tissues. Comparison with flow cytometric analysis. *Am J Pathol* 134:733–739, 1989
34. WOOLLET GR, BARCLAY AN, PUKLAVEC M, WILLIAMS AF: Molecular and antigenic heterogeneity of the rat leukocyte-common antigen from thymocytes and T and B lymphocytes. *Eur J Immunol* 15:168–173, 1985
35. DIJKSTRA CD, DÖPP EA, JOLING P, KRAAL G: The heterogeneity of mononuclear phagocytes in lymphoid organs: Distinct macrophage subpopulations in the rat recognized by monoclonal antibodies ED1, ED2, and ED3. *Immunology* 54:589–599, 1985
36. BRIDEAU RJ, CARTER PB, MCMASTER WR, MASON DW, WILLIAMS AF: Two subsets of rat T lymphocytes defined with monoclonal antibodies. *Eur J Immunol* 10:609–615, 1980
37. MCMASTER WR, WILLIAMS AF: Identification of Ia glycoproteins in rat thymus and purification from rat spleen. *Eur J Immunol* 9:426–433, 1979
38. DECLERCK PJ, ALESSI M-C, VERSTREKEN M, KRUITHOF EKO, JUHAN-VAGUE I, COLLEN D: Measurement of plasminogen activator inhibitor 1 in biological fluids with a murine monoclonal antibody-based enzyme-linked immunosorbent assay. *Blood* 71:220–225, 1988
39. VERPOOTEN GA, WYBO I, PATTYN VM, HENDRIX PG, GIULIANO RA, NOUWEN EJ, ROELS F, DE BROE ME: Cyclosporine nephrotoxicity: Comparative cytochemical study of rat kidney and human allograft biopsies. *Clin Nephrol* 25(Suppl 1):S18–S22, 1986
40. KOPP JB, KLOFMAN PE: Cellular and molecular mechanisms of cyclosporin nephrotoxicity. *J Am Soc Nephrol* 1:162–179, 1990
41. KAPLAN R, AYNEDJIAN HS, SCHLONDORFF D, BANK N: Renal vasoconstriction caused by short-term cholesterol feeding is corrected by thromboxane antagonist or probucol. *J Clin Invest* 86:1707–1714, 1990
42. GUPTA SK, BENET LZ: High-fat meals increase the clearance of cyclosporine. *Pharmaceutical Res* 7:46–48, 1990
43. HORTON JD, CUTHBERT JA, SPADY DK: Regulation of hepatic 7α-hydroxylase expression and response to dietary cholesterol in the rat and hamster. *J Biol Chem* 270:5381–5387, 1995
44. VLAHCEVIC ZR, HEUMAN DM, HYLEMON PB: Regulation of bile acid synthesis. *Hepatology* 13:590–600, 1991
45. CHOICE E, MASIN D, BALLY MB, MELOCHE M, MADDEN TD: Liposomal cyclosporine. Comparison of drug and lipid carrier pharmacokinetics and biodistribution. *Transplantation* 60:1006–1011, 1995
46. EDDY AA, LIU E, MCCULLOCH L: Interstitial inflammation and fibrosis in rats with diet-induced hypercholesterolemia. *Kidney Int* 50:1139–1149, 1996
47. SHIVJI MKK, KENNY MK, WOOD RD: Proliferating cell nuclear antigen is required for DNA excision repair. *Cell* 69:367–374, 1992
48. KONE BC, RACUSEN LC, WHELTON A, SOLEZ K: Acute renal failure produced by combining cyclosporine and brief renal ischemia in the Munich Wistar rat. *Clin Nephrol* 25(Suppl 1):S171–S174, 1986
49. LAN HY, MU W, NIKOLIC-PATERSON DJ, ATKINS RC: A novel, simple, reliable, and sensitive method for multiple immunoenzyme staining: Use of microwave oven heating to block antibody crossreactivity and retrieve antigens. *J Histochem Cytochem* 43:97–102, 1995
50. KOVACS EJ: Fibrogenic cytokines: The role of immune mediators in the development of scar tissue. *Immunol Today* 12:17–23, 1991
51. AYA N, YOSHIOKA K, MURAKAMI K, HINO S, OKADA K, MATSUO O, MAKI S: Tissue-type plasminogen activator and its inhibitor in human glomerulonephritis. *J Pathol* 166:289–295, 1992
52. RONDEAU E, MOUGENOT B, LACAVE R, PERALDI MN, KRUITHOF EKO, SRAER JD: Plasminogen activator inhibitor 1 in renal fibrin deposits of human nephropathies. *Clin Nephrol* 33:55–60, 1990
53. EDDY AA, GIACHELLI CM, MCCULLOCH L, LIU E: Renal expression of genes that promote interstitial inflammation and fibrosis in rats with protein-overload proteinuria. *Kidney Int* 47:1546–1557, 1995
54. TOMOOKA S, BORDER WA, MARSHALL BC, NOBLE NA: Glomerular matrix accumulation is linked to inhibition of the plasmin protease system. *Kidney Int* 42:1462–1469, 1992
55. BARNES JL, MITCHELL RJ, TORRES ES: Expression of plasminogen activator-inhibitor-1 (PAI-1) during cellular remodeling in proliferative glomerulonephritis in the rat. *J Histochem Cytochem* 43:895–905, 1995
56. KEETON M, EGUCHI Y, SAWDEY M, AHN C, LOSKUTOFF DJ: Cellular localization of type 1 plasminogen activator inhibitor messenger RNA and protein in murine renal tissue. *Am J Pathol* 142:59–70, 1993
57. GINSBERG D, ZEHEB R, YANG AY, RAFFERTY UM, ANDREASEN PA, NIELSEN L, DANO K, LEBO RV, GELEHRTER TD: cDNA cloning of human plasminogen activator-inhibitor from endothelial cells. *J Clin Invest* 78:1673–1680, 1986
58. HEKMAN CM, LOSKUTOFF DJ: Endothelial cells produce a latent inhibitor of plasminogen activators that can be activated by denaturants. *J Biol Chem* 260:11581–11587, 1985
59. DEBROCK S, DECLERCK PJ: Characterization of common neoantigenic epitopes generated in plasminogen activator inhibitor-1 after cleavage of the reactive center loop or after complex formation with various serine proteinases. *FEBS Lett* 376:243–246, 1995
60. MADSEN KM, BRENNER BM: Structure and function of the renal tubule and interstitium, in *Renal Pathology*, edited by TISCHER CC, BRENNER BM, Philadelphia, JB Lippincott Company, 1989, pp 1518–1551
61. NYKJAER A, PETERSEN CM, MOLLER B, JENSEN PH, MOESTROP SK, HOLTET TL, ETZERODT M, THOGERSEN HC, MUNCH M, ANDREASEN PA, GLIEMANN J: Purified α2-macroglobulin receptor/LDL receptor-related protein binds urokinase plasminogen activator inhibitor type-1 complex. *J Biol Chem* 267:14543–14546, 1992
62. CHRISTENSEN EI, NIELSEN S, MOESTRUP SK, BORRE C, MAUNSBACH AB, DE HEER E, RONCO P, HAMMOND TG, VERROUST P: Segmental distribution of the endocytosis receptor gp330 in renal proximal tubules. *Eur J Cell Biol* 66:349–364, 1995
63. PREISSNER KT: Structure and biological role of vitronectin. *Annu Rev Cell Biol* 7:275–310, 1991
64. WANG Y, THOMPSON EM, WHAWELL SA, FLEMING KA: Expression and localization of plasminogen activator inhibitor 1 mRNA in transplant kidneys. *J Pathol* 169:445–450, 1993
65. EDDY AA: Expression of genes that promote renal interstitial fibrosis in rats with proteinuria. *Kidney Int* 49(Suppl 54):S49–S54, 1996